Overcoming Systematic Effects in Ring-Diagram Fitting

Richard Bogart[1], Charles Baldner[1], & Sarbani Basu[2]

1: Stanford University; *2:* Yale University

Abstract

Although the principles involved in understanding ring-diagram mode frequencies are well understood, the procedures for determining those frequencies in the power spectra of flattened geometries are plagued by several systematic effects which are not well understood. It is possible to overcome these effects in certain cases by comparing inversions of the fitted mode parameters, or just the parameters themselves, for particular targets with those for otherwise similar targets. We can thus draw useful information about features localized in both space and time, such as regions of anomalous flows or the thermal structures of active regions. But reliable measurements of the large-scale or long-term mean dynamical structure of the near-surface regions, particularly the profiles of differential rotation and meridional circulation, may require more robust estimations of the mode parameters than are presently available. We describe the known systematic effects in the extensive ring-diagram analysis of HMI Doppler data and explore some methods of overcoming or dealing with them.

The measured flows exhibit consistent variations across the effective position on the disk, including east-west asymmetries on average that cannot be real. The structures are very similar for data from different sources (Fig. 1). When power spectra from different times at the same location are averaged together, the same disc-position variations in the ring-fit flow parameters are manifested (Fig. 2) strongly suggesting that the systematics are in the analysis procedure. By simply removing the long-term means at each disc position, small but apparently significant features localized in space and/or time as residuals can be observed (Figure 3, and talk by Baldner). For reliable measurements of the mean differential rotation, including the near-surface shear layer, and in particular the meridional circulation, however, the spatial systematics must be better characterized and understood.

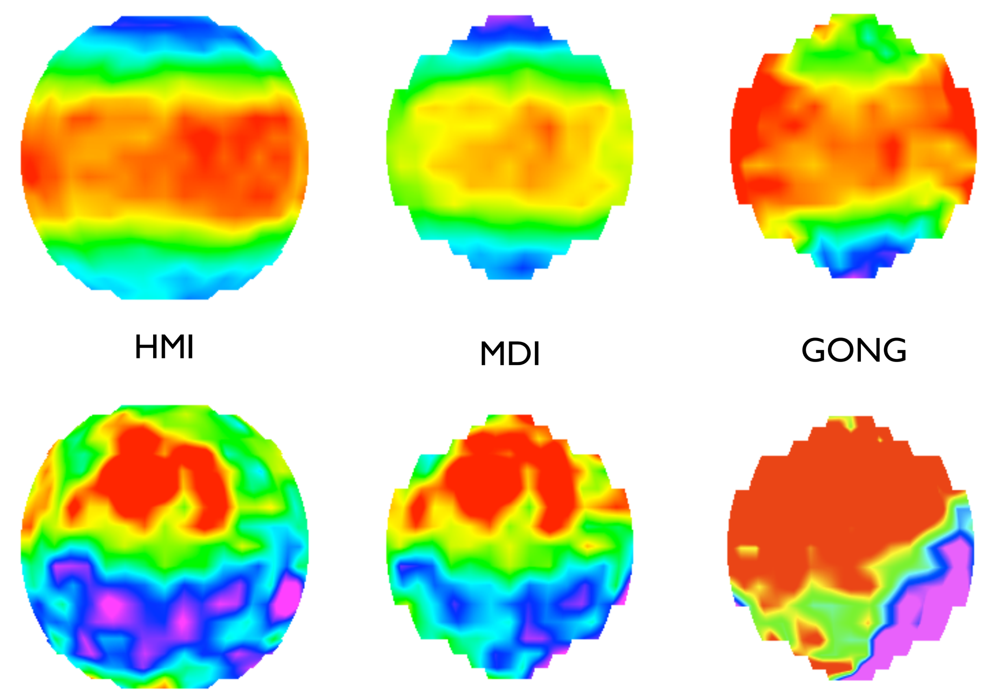

Figure 1. Spatial distribution of the U_x (zonal flow, above) and U_y (meridional flow) parameters on day 2097:180 (2.6 June 2010), from "fast" fits, in the near-surface range of modes ($2 < \nu$ [μHz] $/ l < 4$: $r_t > 0.995$ R$_\odot$)

"HMI as MDI" analysis used HMI data interpolated to a cadence of 60-sec and mapped to a resolution of 0°12/pxl in the same target locations as used for the MDI and GONG ring-diagram pipelines.

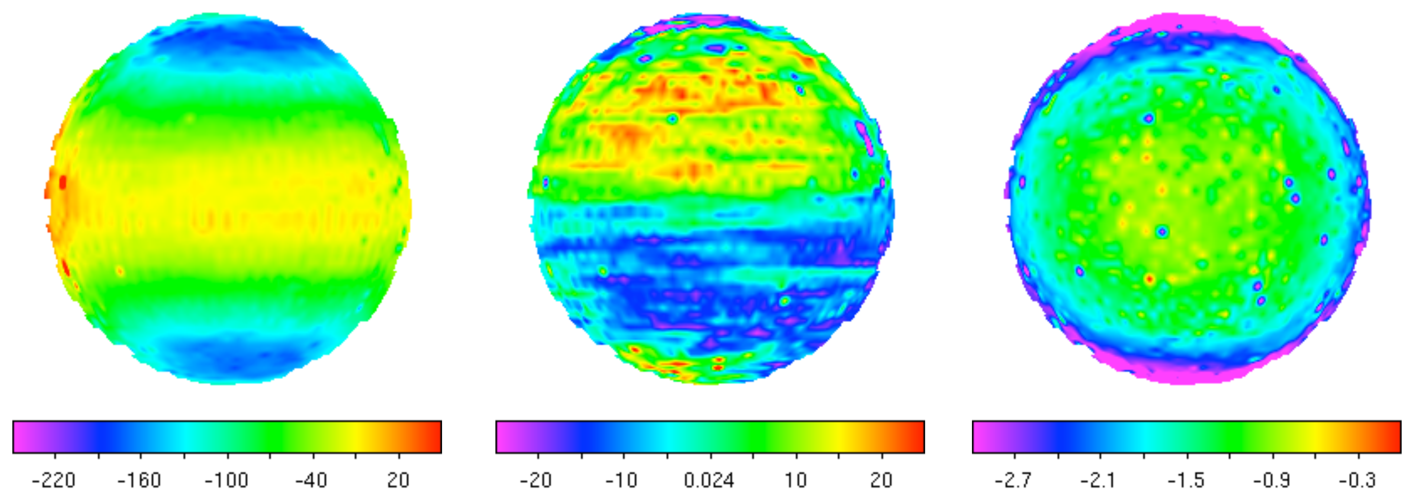

Figure 2. Spatial distribution of the U_x, (left), U_y (middle), and A_0 (mode amplitude) parameters averaged over CR 2164 (May–June 2015), from the "comprehensive" fits to HMI data, for the same near-surface range of modes as in Fig. 1, with radial orders n = 1–4.

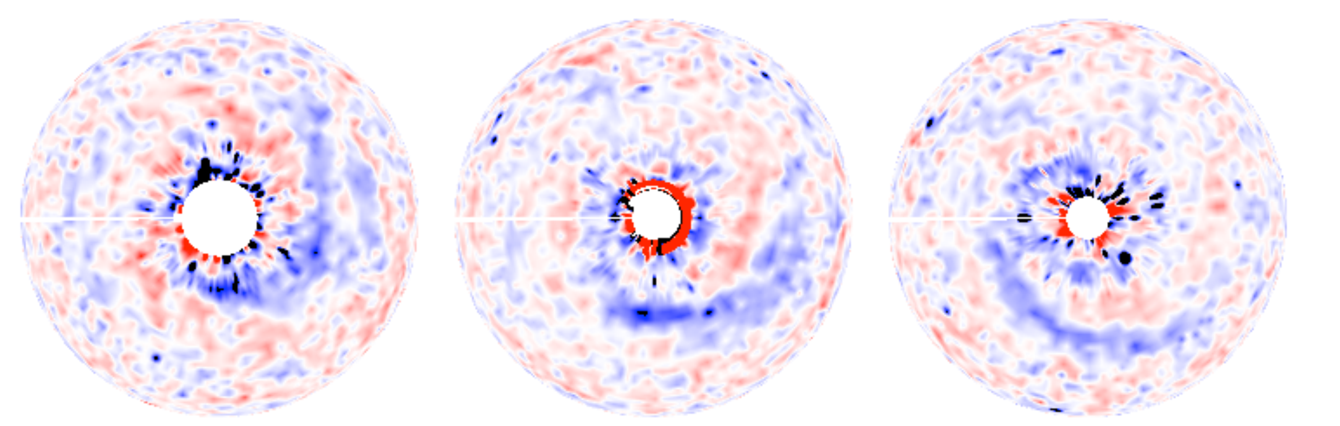

Figure 3. Polar views of the northern hemisphere residuals from the mean flows U_x at each location for the three succesive rotations CR 2097–2099. The color scale range is ±0.5 m/s.

Fitting to Averaged Spectra

Instead of averaging inverted flow results or the mode fit parameters for the same disc position observed at different times, we can average the power spectra and fit those, since the peaks in the ring-diagram regime are broad and the modes incoherent anyway. The spectra for the HMI 15˚ and 30˚ analysis regions have been routinely averaged together for each location over each rotation (24 or 12 instances for each of ~280 or 69 regions respectively) since start of mission, and we have recently started averaging together the spectra for the 5˚ regions as well (72 instances for each of ~2750 regions per rotation.) Figure 4 shows sample fits of the U_x parameter to rotation-averaged spectra at different latitudes, reflecting differential rotation.

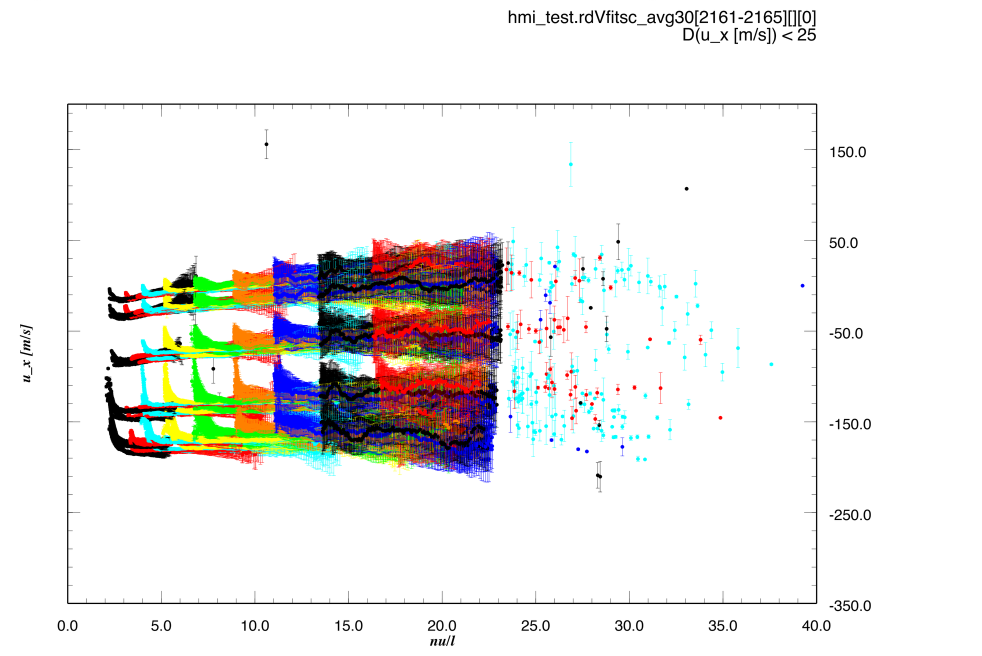

Figure 4. The zonal flow parameter U_x for all mode fits to the rotation-averaged spectra of 30˚ regions at latitudes 0˚, ±15˚, ±30˚, ±45˚, and ±60˚ on central meridian for five rotations CR 2161–2165 (Mar–July 2015).

Fitting the Background Power

Both ring fitting procedures fit Lorentzian profiles with a background term assumed to vary as k^{-3}, mainly to account for the contributions of neighboring modes. The "comprehensive" one fits for a second background term assumed to vary as k^{-4} as well. Fig. 5 shows examples of composite background spectra, constructed from the contributions of the background fit terms where mode fits exist, and the original power where there are no mode fits. Since the background power in the well-separated inter-ridge regions is well below that along the ridges, it appears that the background power along the ridges is being substantially overestimated.

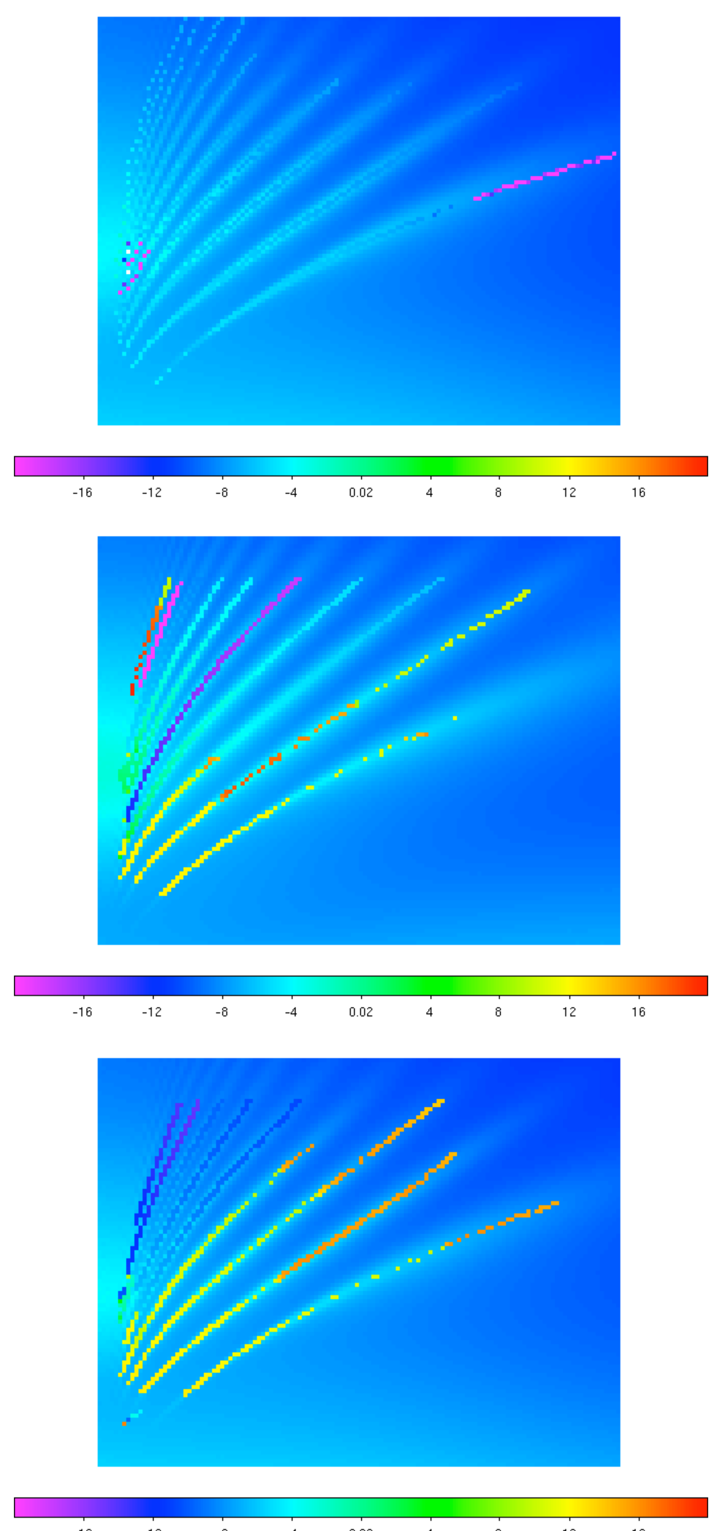

Figure 5. "Reconstructed" background power spectra from the fits to the averaged 30˚ spectra for CR 2164 on the central meridian at latitude +60˚ (top), 0˚ (middle), and -60˚ (bottom).

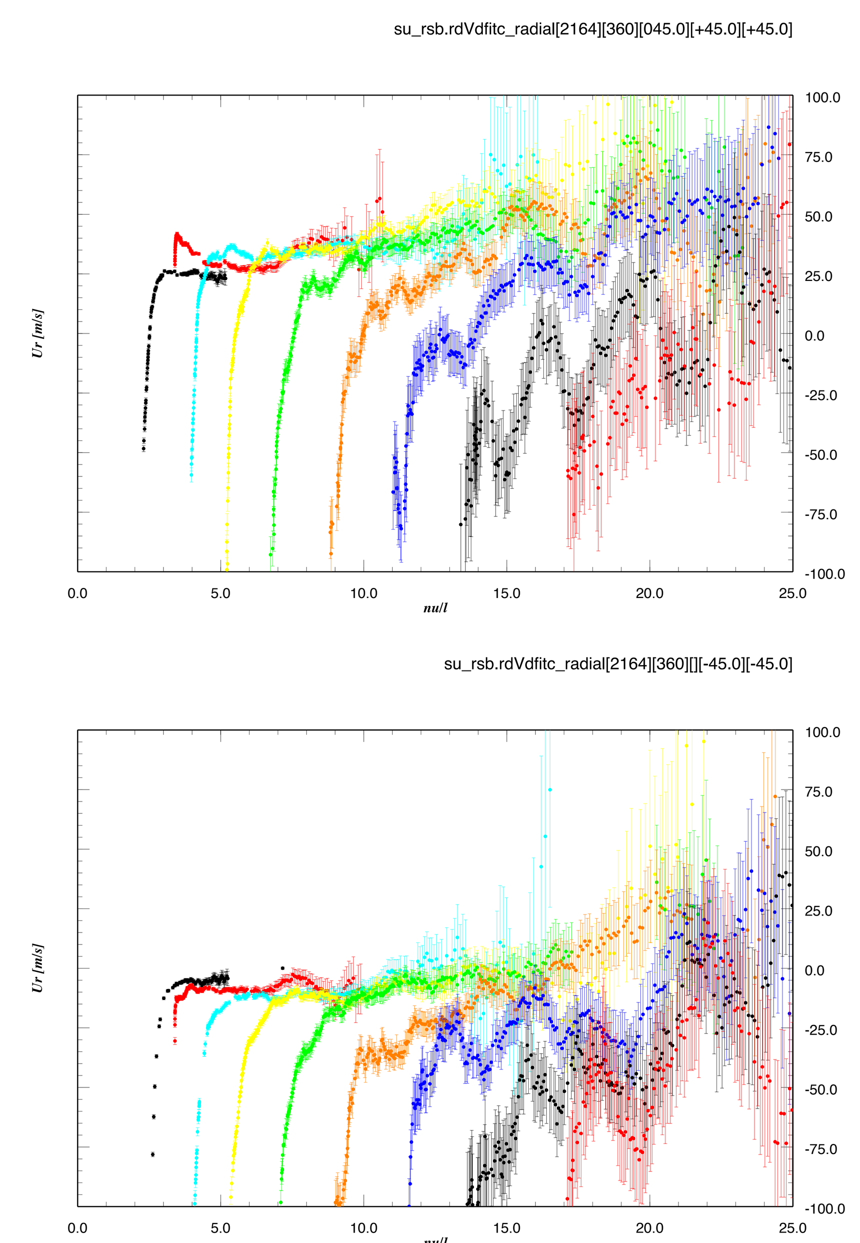

Figure 7. Mode fits for the "radial flow" parameter U_r vs classical turning point at two sample locations in the northwest quadrant (above) and southeast (below), for one time sample (2164:360, 21 May 2015). Different radial orders are distinguished by color.

Is There a Radial Pseudo-Flow?

The measured east-west asymmetry in the inferred zonal flow at the equator when the latitude of disc center is close to 0 has been used as a proxy for an assumed general radial component of the flows as an artifact of the data analysis. We have attempted to determine how much of this asymmetry is due to a radial component and how much to a genuine east-west asymmetry. Since the zonal flow is not strictly along geodesics, and in any case normally includes a very large component due to uncompensated differential rotation in the tracking, we have retracked the regions in coördinate frames in which the horizontal axes are parallel to and perpendicular to the direction from disc center to the center of each region at the middle of the tracking interval. For such an analysis, it is of course necessary to remove the large first-order zonal flow due to rotation, so we have tracked at a rate that removes the mean measured values of the zonal flow parameter U_x near the surface. The rate we use is the average for the first four years of HMI data, for a depth of ~5 Mm (r/R_0=0.9925±0.005). The difference between this rate and the nominal photospheric Doppler rotation profile is shown in Fig. 6. In the analysis, one U term represents advection in the radial direction, and the other in the transverse (circumferential) direction. Two samples of the "U_r" fits are shown in Fig. 7. Their spatial variation is shown for an analysis of six 57.6-hour intervals during a recent rotation with $B_0 \approx 0$ in Figs. 8 & 9. It seems clear from these that the east-west term greatly dominates over any radial term (which would be uniform in position angle around the limb); that it does not vary greatly from center of disc to the limb and is consequently not predominantly a center-to-limb effect; and that its amplitude increases significantly with depth, so it is not just a reflection of the tracking rate. Likewise, the regular variation of the "circumferential" flow around the limb is consistent with a flow effect in a single direction; a "washing machine" effect would produce a constant circumferential signal.

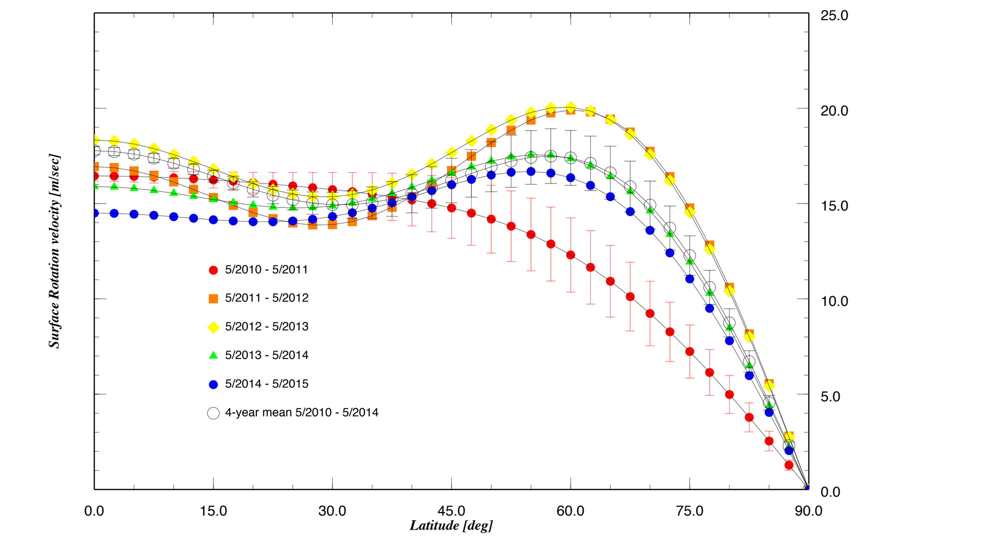

Figure 6. Differences between the surface velocity for the best-fit differential rotation profiles for modes at a depth of 0.9925±0.005 r/R_0 and the standard photospheric Doppler rate at the same latitude, for each year of the HMI mission. The average for the first four years, used in the analysis here, is represented by the open circles.

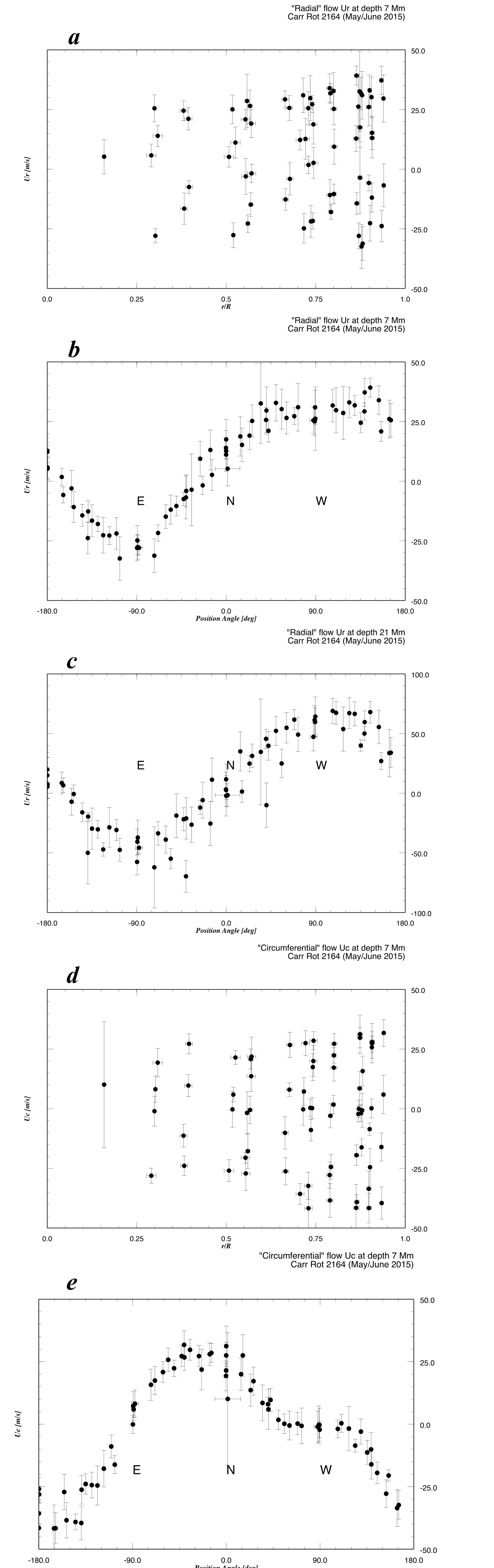

Figure 8. (5 graphs at the right). Variation of the inverted radial flow component U_r (*a*–*c*) and the tangential or circumferential flow compnent U_c (*d*–*e*) vs. center-to-limb distance (*a*,*d*) and position angle (*b*,*c*,*e*), at target depths of 0.99 R_0 (*a*,*b*,*d*,*e*) and 0.97 R_0 (*c*).

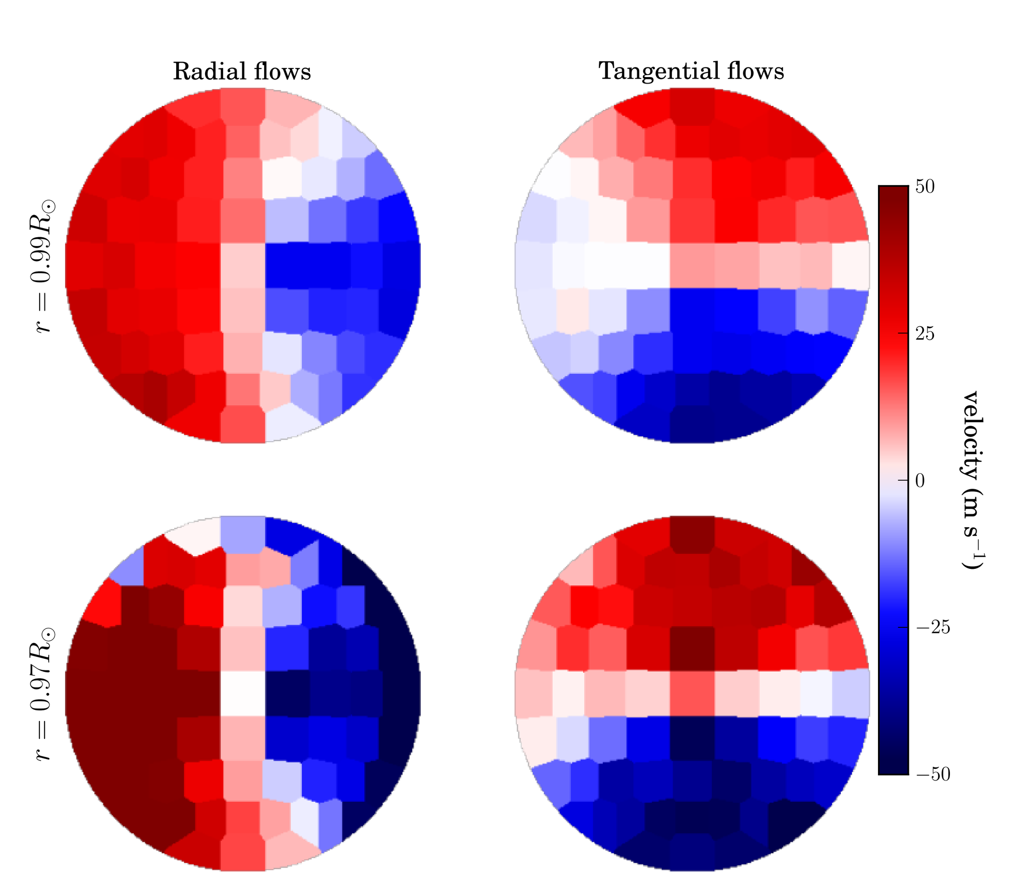

Figure 9. (4 maps at the right, bottom). Spatial maps showing the same radial and circumferential (tangential) flows at two target depths as in Figure 7. (N.B. maps are inverted, west on the left.)